Entanglement on an optical atomic-clock transition

https://doi.org/10.1038/s41586-020-3006-1

Received: 12 June 2020

Accepted: 21 October 2020

Published online: 16 December 2020

Check for updates

Edwin Pedrozo-Peñafiel[1,7], Simone Colombo[1,7], Chi Shu[1,2,7], Albert F. Adiyatullin[1], Zeyang Li[1], Enrique Mendez[1], Boris Braverman[1,5], Akio Kawasaki[1,6], Daisuke Akamatsu[1,3], Yanhong Xiao[1,4] & Vladan Vuletić[1]✉

State-of-the-art atomic clocks are based on the precise detection of the energy difference between two atomic levels, which is measured in terms of the quantum phase accumulated over a given time interval[1–4]. The stability of optical-lattice clocks (OLCs) is limited both by the interrupted interrogation of the atomic system by the local-oscillator laser (Dick noise[5]) and by the standard quantum limit (SQL) that arises from the quantum noise associated with discrete measurement outcomes. Although schemes for removing the Dick noise have been recently proposed and implemented[4,6–8], performance beyond the SQL by engineering quantum correlations (entanglement) between atoms[9–20] has been demonstrated only in proof-of-principle experiments with microwave clocks of limited stability. The generation of entanglement on an optical-clock transition and operation of an OLC beyond the SQL represent important goals in quantum metrology, but have not yet been demonstrated experimentally[16]. Here we report the creation of a many-atom entangled state on an OLC transition, and use it to demonstrate a Ramsey sequence with an Allan deviation below the SQL after subtraction of the local-oscillator noise. We achieve a metrological gain of $4.4^{+0.6}_{-0.4}$ decibels over the SQL by using an ensemble consisting of a few hundred ytterbium-171 atoms, corresponding to a reduction of the averaging time by a factor of 2.8 ± 0.3. Our results are currently limited by the phase noise of the local oscillator and Dick noise, but demonstrate the possible performance improvement in state-of-the-art OLCs[1–4] through the use of entanglement. This will enable further advances in timekeeping precision and accuracy, with many scientific and technological applications, including precision tests of the fundamental laws of physics[21–23], geodesy[24–26] and gravitational-wave detection[27].

Progress in atomic, optical and quantum physics over the past decades has boosted the performances of OLCs to an astonishing fractional accuracy near 10^{-18} (refs. [1–4]). Recently, technical noise in some OLCs has been reduced to near or below the level of the intrinsic quantum noise[3,4]. A clock operated with N uncorrelated atoms for an averaging time τ at the SQL can reach a quantum noise-limited fractional stability given by

$$\sigma(\tau_R, \tau) = \frac{1}{\omega_0 \tau_R}\sqrt{\frac{T_c}{\tau}}\sqrt{\frac{\xi_W^2}{N}}, \quad (1)$$

where τ_R is the interrogation time (Ramsey time) of the atoms by the clock local oscillator laser, T_c the clock cycle time, ω_0 the angular frequency of the clock transition, and the Wineland parameter is $\xi_W^2 = 1$ (ref. [28]) for ideal conditions with perfect quantum coherent state preparation and detection. If the clock is operated at a duty cycle less than 1 ($T_c > \tau_R$), so that the local oscillator is not locked to the atomic evolution during part of the cycle, then the Dick noise σ^2_{Dick}, which arises from aliased high-frequency noise of the local oscillator, should be added to equation (1) [5,6]. The Dick noise can be suppressed by using two ensembles to eliminate the dead time[4,6] or by performing simultaneous interrogation of two ensembles[7,8].

The SQL, as described by equation (1) with $\xi_W^2 = 1$, is not a fundamental limit, but can be overcome by means of quantum correlations (entanglement) between the participating atoms. The simplest entangled state offering metrological gain is the squeezed spin state (SSS)[29], where the quantum noise is redistributed between two orthogonal spin quadratures, one with reduced quantum noise (squeezed axis) and the other with increased noise (anti-squeezed axis); see Fig. 1d. In this picture, each atom is associated with a spin of 1/2, and the N-atom ensemble with a collective spin of $S_0 = N/2$. By orienting the squeezed quadrature

[1]Department of Physics, MIT-Harvard Center for Ultracold Atoms and Research Laboratory of Electronics, Massachusetts Institute of Technology, Cambridge, MA, USA. [2]Department of Physics, Harvard University, Cambridge, MA, USA. [3]National Metrology Institute of Japan (NMIJ), National Institute of Advanced Industrial Science and Technology (AIST), Tsukuba, Japan. [4]State Key Laboratory of Quantum Optics and Quantum Optics Devices, Institute of Laser Spectroscopy, and Collaborative Innovation Center of Extreme Optics, Shanxi University, Taiyuan, China. [5]Present address: Department of Physics and Max Planck Centre for Extreme and Quantum Photonics, University of Ottawa, Ottawa, Ontario, Canada. [6]Present address: W. W. Hansen Experimental Physics Laboratory and Department of Physics, Stanford University, Stanford, CA, USA. [7]These authors contributed equally: Edwin Pedrozo-Peñafiel, Simone Colombo, Chi Shu. ✉e-mail: vuletic@mit.edu

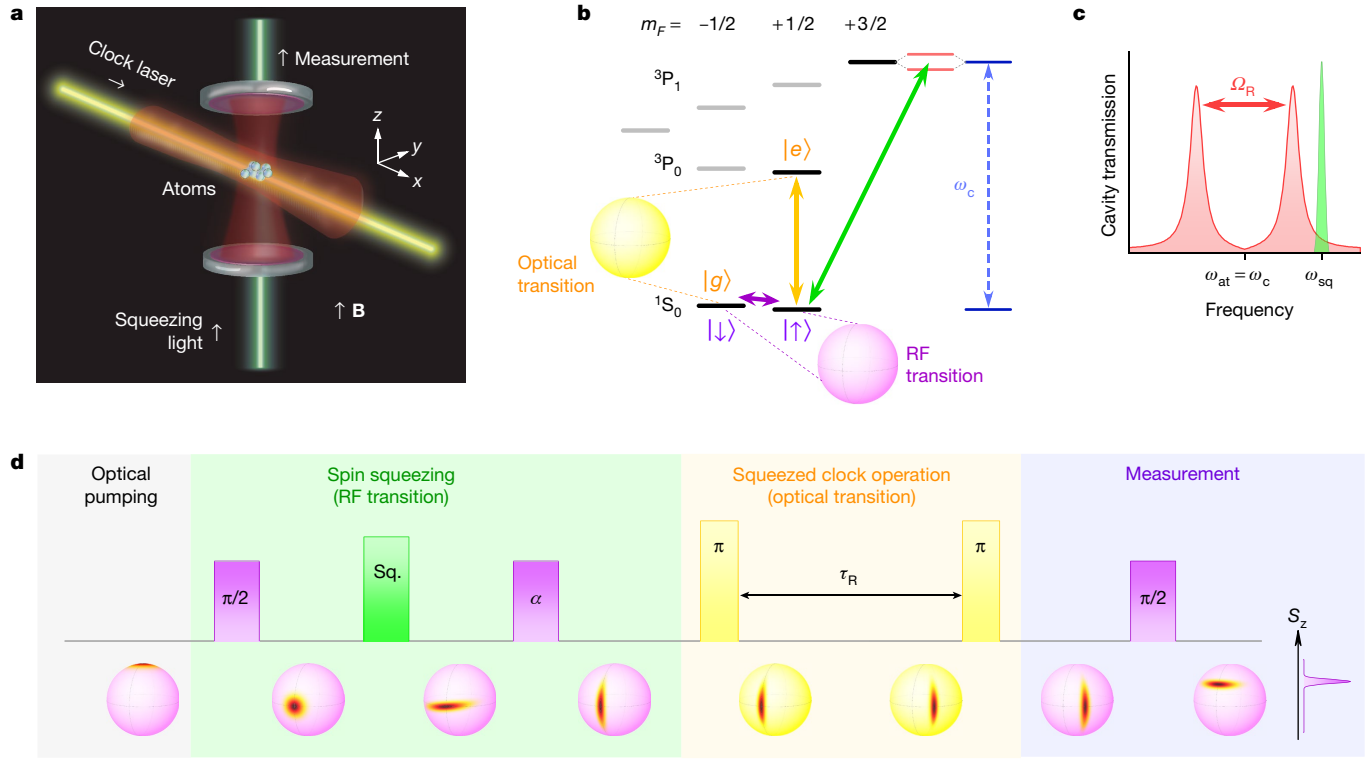

Fig. 1 | Setup and squeezed-clock sequence. a, ^{171}Yb atoms are trapped inside an optical cavity in a two-dimensional magic-wavelength optical lattice along the x and z directions (red). Light for optical pumping and spin squeezing (green) is applied along the cavity axis z while the clock laser (yellow) propagates along x. **b**, Energy levels and transitions. Purple, green and yellow pulses indicate the ground-state RF transition $|\downarrow\rangle \rightarrow |\uparrow\rangle$, the squeezing transition $|^1S_0, m_I = 1/2\rangle \rightarrow |^3P_1, m_F = 3/2\rangle$ at ω_{at} and the optical-clock transition $|\uparrow\rangle \rightarrow |e\rangle$, respectively. The system evolves either in the ground-state manifold $\{|\downarrow\rangle, |\uparrow\rangle\}$ (purple Bloch sphere) or in the clock-state manifold $\{|g\rangle, |e\rangle\}$ (yellow Bloch sphere). The cavity frequency ω_c is tuned in resonance with the squeezing transition, $\omega_c = \omega_{at}$. **c**, Spin squeezing. Strong coupling of the atoms to the cavity results in vacuum Rabi splitting of the cavity resonance (red peaks). A laser is applied detuned from the Rabi peak at frequency ω_{sq} (green peak) to produce an SSS via cavity feedback[20]. **d**, Squeezed-clock sequence. An SSS is prepared in the ground-state manifold $\{|\downarrow\rangle, |\uparrow\rangle\}$ and rotated by an angle α, transferred to the clock manifold $\{|g\rangle, |e\rangle\}$, evolved in a Ramsey sequence for time τ_R, and mapped back onto $\{|\downarrow\rangle, |\uparrow\rangle\}$, where a state measurement is performed. The evolution of the quantum state is depicted on the Bloch spheres for the RF (purple) and optical (yellow) transitions.

of the collective spin along the phase axis during clock operation, one can reduce the quantum noise and increase the clock stability. The potential metrological gain over the SQL, expressed in variance, is then given by ξ_W^{-2}, where the Wineland parameter $\xi_W^2 = \xi^2/C^2$ (ref. [28]; C is the contrast) incorporates both the the variance reduction ξ^2 of the spin noise compared to an unentangled coherent spin state (CSS) and the magnitude of the mean spin vector, $|\langle \mathbf{S} \rangle| = CS_0$.

Over the past decade, SSSs have been demonstrated in several systems[16], including atomic Bose–Einstein condensates[11,12,15,30], cold atomic ensembles[9,10,13,14,17,20] and trapped ions[19]. In neutral atoms, up to 20 dB of spin squeezing beyond the SQL has been demonstrated using optical techniques[17,18]. However, given that it is more difficult to maintain phase coherence at high frequencies, all spin squeezing so far has involved transitions with frequencies ω_0 5–10 orders of magnitude smaller than optical frequencies, and that exhibit proportionally reduced time-keeping precision (see equation (1)). Building on spin-squeezing generation between nuclear sublevels of the electronic ground state of ^{171}Yb that we have recently demonstrated[20], here we report the generation of an SSS on an optical transition and demonstrate an OLC in which the atomic system can provide sensitivity beyond the SQL.

Our clock operates with an ensemble of $N = 350 \pm 40$ ^{171}Yb atoms (all uncertainties are 1σ statistical errors) that are confined in a two-dimensional magic-wavelength optical-lattice trap inside a high-finesse ($\mathcal{F} \approx 12,000$) optical cavity[20] (see Fig. 1a) and are Raman-sideband-cooled to mean vibrational quantum number $\langle n_x \rangle < 0.2$. In order to robustly create an SSS on the ultra-narrow optical-clock transition, we first generate spin squeezing between the two nuclear sublevels $|\uparrow\rangle = |^1S_0, m_I = +1/2\rangle$ and $|\downarrow\rangle = |^1S_0, m_I = -1/2\rangle$ of the electronic ground state $^1S_0$ using the interaction between the atoms and the optical cavity[14,20]. Subsequently, we transfer the population of $|\uparrow\rangle$ into the $|e\rangle = |^3P_0, m_I = 1/2\rangle$ excited clock state with a π pulse of the clock laser, thereby mapping the SSS onto the optical-clock manifold $\{|g\rangle |e\rangle\}$, where $|g\rangle = |\downarrow\rangle$ and m_I indicates the nuclear spin sublevel (see Fig. 1b).

The spin squeezing between the ground-state sublevels is achieved by optically pumping the atoms into state $|\uparrow\rangle$, creating a CSS between $|\uparrow\rangle$ and $|\downarrow\rangle$ with a radiofrequency (RF) π/2 pulse, and then applying a laser pulse near the $|\uparrow\rangle = |^3P_1, m_F = 3/2\rangle$ transition through the cavity[20] (Fig. 1c), where m_F indicates the Zeeman sublevel of the $^3P_1$ state. The atom–light interaction, amplified by the cavity, approximates the one-axis twisting Hamiltonian[29] with longitudinal magnetic field, $H_1 = \beta S_z + \chi S_z^2$, where β is the light-shift parameter and χ the shearing parameter. A spin-echo protocol is then used to cancel the linear term (S_z), so that the system evolves under an effective one-axis twisting Hamiltonian $H = \chi S_z^2$ (refs. [20,29]) for a time τ_s (see Methods and Fig. 1d). Finally, the reduced spin-projection noise can be oriented along any desired axis in the $\{|\downarrow\rangle, |\uparrow\rangle\}$ ground-state manifold by rotating the SSS around its average spin direction $\langle \mathbf{S} \rangle$ with another RF pulse. At this stage, we observe a spin-noise suppression of $\xi_-^2 = 6$ dB—limited by the state detection (see Methods), with an intrinsic spin noise reduction of 9 dB—and a contrast of $C = 0.97$. The SSS is nearly uncertainty-limited, with a detected area 1.9 times larger than the limit set by Heisenberg's uncertainty principle[20].

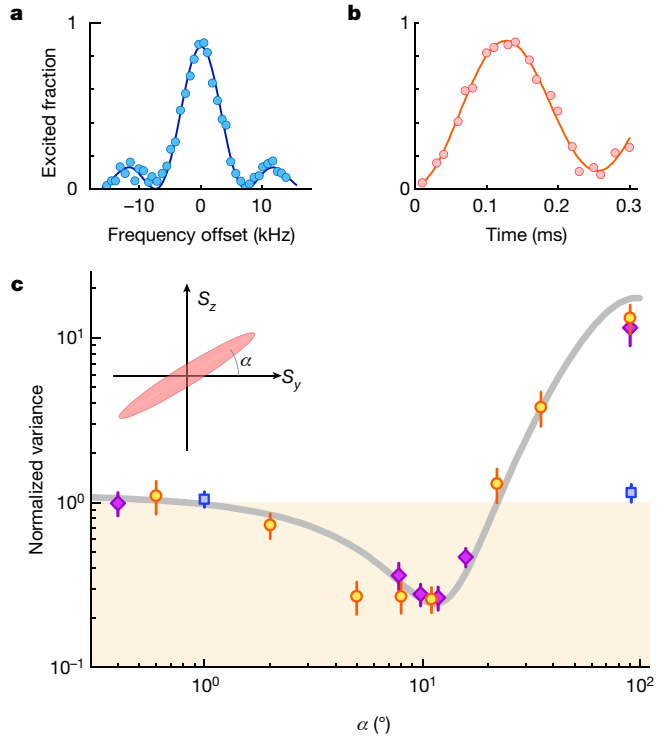

Fig. 2 | Squeezed state tomography. a, Rabi spectroscopy of the $n_x \rightarrow n_x$ vibrational component of the $|\uparrow\rangle \rightarrow |e\rangle$ transition to the clock state. The pulse duration is 0.22 ms. The solid line is a guide for the eye. **b**, Rabi oscillations on the clock transition. The data are fitted with a damped oscillator model (solid line). **c**, Tomographic measurements of the SSS before (purple diamonds) and after (orange circles) mapping onto the clock transition and back, which show very similar degrees of squeezing. The theoretical expectation for a state with $\xi^2_- = -5.9$ dB is shown as a grey solid line. Two measured data points for a CSS are also shown (blue squares). The shaded area indicates the region below the SQL. Error bars represent 1σ statistical confidence interval.

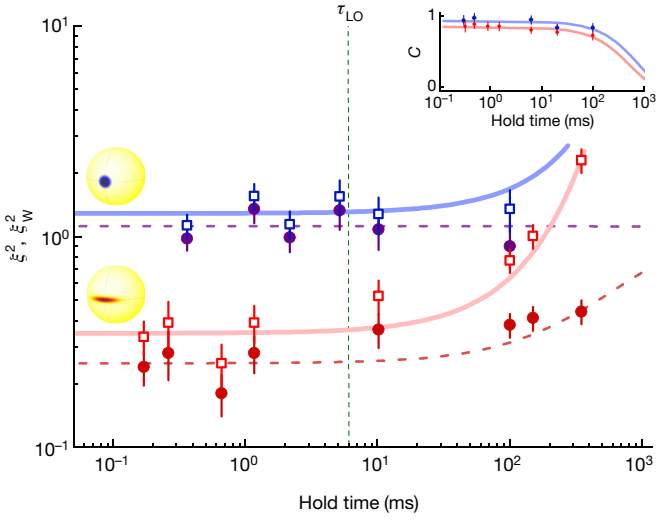

Fig. 3 | Spin noise and Wineland parameter of the clock transition as a function of time. The measured normalized S_z spin noise ξ^2 (solid circles) and model (dashed lines) for the CSS (purple) and the SSS with the squeezed axis aligned along S_z (dark red) increases slowly with time. The increase is caused by the finite 800-ms lifetime of the state $|e\rangle$ due to scattering of the trapping light. The Wineland parameter ξ^2_W (open squares) depends in addition on the contrast loss due to shortening of the atomic collective spin $|\langle \mathbf{S} \rangle|$ (inset; blue data points for CSS, red data points for SSS, with exponential fits). The solid lines represent the Wineland parameter predicted using the fit to the measured contrast. τ_{LO} indicates the coherence time of the local oscillator. Error bars represent 1σ statistical confidence interval.

Having prepared an SSS in the $\{|\uparrow\rangle, |\downarrow\rangle\}$ ground-state manifold, we then map it onto the optical-clock transition $^1S_0 \rightarrow {}^3P_0$ by phase-coherently transferring the population of $|\uparrow\rangle$ to the state $|e\rangle$ with an optical π pulse of the local oscillator. We observe a clean Rabi spectrum on the $|g\rangle \rightarrow |e\rangle$ transition (Fig. 2a) and coherent Rabi oscillations in time (Fig. 2b). The π pulse has a transfer efficiency of 0.95, which is mostly limited by the finite atomic temperature. This efficiency sets a limit on the observable noise reduction of 13 dB below the projection noise limit, and thus we do not expect any substantial degradation of the spin squeezing to arise from mapping the SSS onto the $|g\rangle \rightarrow |e\rangle$ clock transition.

We first demonstrate that the entanglement survives the transfer $|g\rangle \rightarrow |e\rangle \rightarrow |g\rangle$ by characterizing the spin squeezing that remains after this process in the $\{|\uparrow\rangle, |\downarrow\rangle\}$ manifold via state tomography (Fig. 2c). We observe that the squeezed noise dips considerably below the standard quantum limit to a level of $\xi^2 = -5.9^{+0.6}_{-0.8}$ dB, where the given uncertainties are 1σ statistical errors, and is essentially the same before and after the mapping onto the clock levels.

Figure 3 shows the measured normalized spin noise ξ^2 and Wineland parameter ξ^2_W as a function of Ramsey time on the optical-clock transition both for a CSS and for an SSS with its squeezed direction oriented along S_z in the $\{|g\rangle, |e\rangle\}$ spin space. In this configuration, which does not improve clock performance but can be used to characterize the entanglement[31], the local-oscillator phase noise does not affect the squeezed quadrature S_z, and we observe that the S_z spin noise remains reduced for times as long as 1 s. While the observed Ramsey contrast decays due to local-oscillator phase noise with a time constant of $\tau_{LO} = 6$ ms, the intrinsic coherence of the atomic state (mean atomic spin vector length $|\langle \mathbf{S} \rangle|$) can be determined even when the local-oscillator phase noise is dominant (see Methods), and the corresponding result is displayed for both the CSS and the SSS in the inset to Fig. 3. The ensemble spin coherence on the optical-clock transition decays exponentially with a time constant of $\tau_{ens} = 0.8 \pm 0.2$ s both for the CSS and the SSS. As Fig. 3 shows, after an interrogation time of about 0.2 s, the SSS is no longer sufficiently entangled to overcome the SQL, but it can still offer metrological gain over the CSS for up to 0.5 s.

In a fully operating atomic clock, the atomic phase is used to stabilize the local-oscillator phase through feedback. Hence, clock performance can be improved by the use of SSSs with the squeezed axis oriented along the phase direction, which allow one to measure the phase difference between atoms and the local oscillator with higher stability than a CSS, and apply correspondingly better feedback[32]. The optimum Ramsey time that achieves maximum gain over the CSS is determined from the local-oscillator coherence time τ_{LO} and the Wineland parameter[33].

In Fig. 4 we demonstrate the implementation of an OLC Ramsey sequence with an entangled-state input, and show that the atomic system provides stability beyond the SQL. We implement the full clock sequence depicted in Fig. 1d with Ramsey times of $\tau_{S1} = 0.17$ ms (Ramsey sequence S1, Fig. 4a) and $\tau_{S2} = 1.16$ ms (Ramsey sequence S2, Fig. 4b). Figure 4a shows that the squeezed clock, although it does not operate beyond its SQL owing to local-oscillator phase noise, has an Allan deviation 3 dB lower than the one operated with a CSS. The local-oscillator phase noise $\Delta\phi_{LO}$ in our system arises predominantly from sequence-to-sequence frequency variations $\Delta\omega/(2\pi) = 78 \pm 3$ Hz of the local oscillator, that is, $\Delta\phi_{LO} = \tau_R \Delta\omega$ (see Methods), and is measured with the sequence S2 with longer Ramsey time. We can then remove $\Delta\phi_{LO}$ from the Allan deviation of the S1 data to obtain the intrinsic stability of the atomic-clock system operated with the SSS at Ramsey time τ_{S1} (red circles in Fig. 4c).

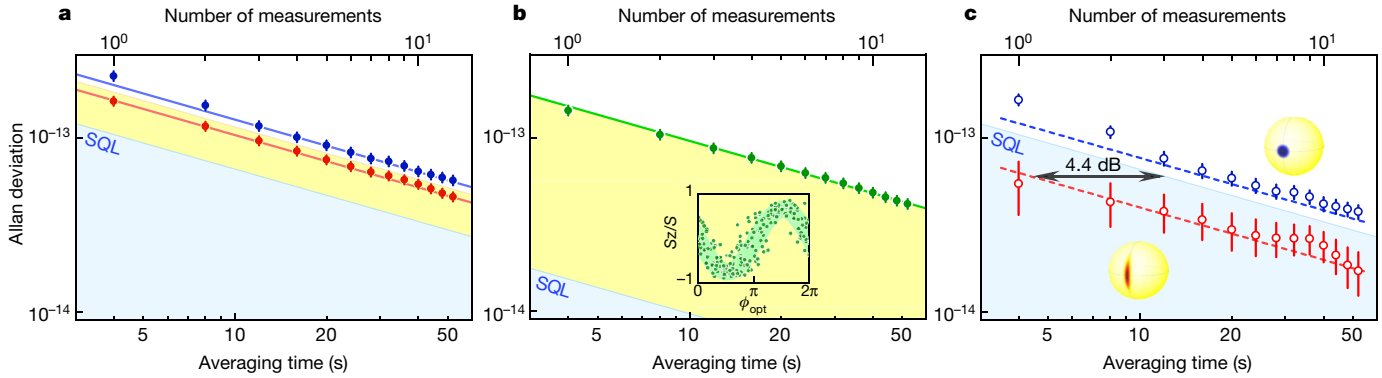

Fig. 4 | Stability improvement with the squeezed clock. a–**c**, The blue shaded area represents the region below the SQL, and the yellow shaded area in **a**, **b** represents the additional contribution from local-oscillator phase noise. **a**, Inferred single-clock cycle stability (self-comparison Allan deviation divided by $\sqrt{2}$)[38] for a CSS (sequence C1, blue) and an SSS (S1, red) with Ramsey time $\tau_{S1} = 0.17$ ms. The squeezed clock operates within the yellow region set by the SQL and local-oscillator phase noise because the quantum projection noise is reduced below the SQL. **b**, Allan deviation for an SSS (sequence S2, green) with a longer Ramsey time of $\tau_{S2} = 1.16$ ms, where the total noise is dominated by the local-oscillator noise. Inset, Ramsey fringes versus local-oscillator phase φ_{opt} of the second Ramsey π pulse for S2. **c**, Data for C1 and S1 after subtraction of the local-oscillator phase noise, where the latter has been calculated from the data for S2 (see Methods). The dashed lines indicate the expected performance estimated from the separately measured Wineland parameter ξ_W^2; see Fig. 3. The other parameters for these measurement are: atom number $N = 300 \pm 30$; single-cycle time $T_c = 4$ s; Ramsey contrast $C_{C1} = 0.91(1)$ for CSS, $C_{S1} = 0.85(1)$ and $C_{S2} = 0.70(1)$ for SSS. Error bars represent 1σ statistical confidence interval.

We further show for comparison a clock operated with a CSS under the same conditions and with the local-oscillator noise also removed (blue circles). The entangled atomic system exhibits a stability that is $4.4^{+0.6}_{-0.4}$ dB below the SQL and 5.7 dB below the CSS, given that the latter is also subject to imperfect state detection and contrast loss. The observed stability improvement due to entanglement is in excellent agreement with that expected from the measured Wineland parameter.

In conclusion, we have generated spin squeezing for many atoms between atomic levels the energies of which differ on the scale of optical photons, and used it to demonstrate an optical-clock sequence in which entanglement provides stability in the atomic system beyond the SQL. Our system is currently limited by local-oscillator phase noise and Dick noise, and reduction of both will be required to fully operate an OLC beyond the SQL. With improvements in local-oscillator stability[1–4] and duty cycles approaching 100%, the Dick noise will be at the same level or smaller than the SQL[6]. Then, a state-of-the-art OLC with 2,000 atoms, Ramsey time of $\tau_R = 2$ s, cycle time of $T_c = 2.3$ s and a contrast of $C = 0.91$ that is limited by the excited-state lifetime, at a metrological gain of 12 dB, which can be obtained by improving the state detection, would reach a fractional stability of $\sigma_{sq} = 1.4 \times 10^{-18} \tau^{-1/2}$ (where the averaging time τ is the expressed in seconds). With further improvements in local-oscillator performance by using novel stabilization schemes[34], we expect no major roadblocks to Ramsey times of tens of seconds using SSSs, and correspondingly improved clock stability in atoms with sufficiently long excited-state lifetime. Moreover, several future fundamental tests based on optical-clock transitions, such as the detection of low-frequency gravitational waves[35] or the search for certain types of dark matter[36], require finite bandwidth of the sensor[35,36]. These applications require short Ramsey time and can fully profit from the sensitivity improvement offered by SSSs. With respect to the Dick noise, some tests of fundamental physics that require the comparison of the transition frequencies between two (or more) atomic ensembles—such as red-shift measurements, gravitational-wave detection, and physics beyond the standard model[23,26,37]—can be performed by interrogating the atomic ensembles simultaneously, thus removing the Dick noise[7,8]. Finally, although possible systematic limitations to the absolute accuracy of the clock due to the presence of the cavity need to be carefully investigated, we anticipate that those adverse effects can be controlled at the level of 10^{-19} or better.

Online content

Any methods, additional references, Nature Research reporting summaries, source data, extended data, supplementary information, acknowledgements, peer review information; details of author contributions and competing interests; and statements of data and code availability are available at https://doi.org/10.1038/s41586-020-3006-1.

1. Ludlow, A. D., Boyd, M. M., Ye, J., Peik, E. & Schmidt, P. O. Optical atomic clocks. *Rev. Mod. Phys.* **87**, 637–701 (2015).
2. Ushijima, I., Takamoto, M., Das, M., Ohkubo, T. & Katori, H. Cryogenic optical lattice clocks. *Nat. Photon.* **9**, 185–189 (2015).
3. Oelker, E. et al. Demonstration of 4.8×10^{-17} stability at 1 s for two independent optical clocks. *Nat. Photon.* **13**, 714–719 (2019).
4. Schioppo, M. et al. Ultrastable optical clock with two cold-atom ensembles. *Nat. Photon.* **11**, 48–52 (2017).
5. Dick, G. J. *Local Oscillator Induced Instabilities in Trapped Ion Frequency Standards*. Report ADA502386 (California Institute of Technology, Pasadena Jet Propulsion Lab, 1987); https://apps.dtic.mil/sti/citations/ADA502386.
6. Norcia, M. A. et al. Seconds-scale coherence on an optical clock transition in a tweezer array. *Science* **366**, 93–97 (2019).
7. Takamoto, M., Takano, T. & Katori, H. Frequency comparison of optical lattice clocks beyond the dick limit. *Nat. Photon.* **5**, 288–292 (2011).
8. Nicholson, T. L. et al. Comparison of two independent Sr optical clocks with 1×10^{-17} stability at 10^3 s. *Phys. Rev. Lett.* **109**, 230801 (2012).
9. Appel, J. et al. Mesoscopic atomic entanglement for precision measurements beyond the standard quantum limit. *Proc. Natl Acad. Sci. USA* **106**, 10960–10965 (2009).
10. Takano, T., Fuyama, M., Namiki, R. & Takahashi, Y. Spin squeezing of a cold atomic ensemble with the nuclear spin of one-half. *Phys. Rev. Lett.* **102**, 033601 (2009).
11. Gross, C., Zibold, T., Nicklas, E., Esteve, J. & Oberthaler, M. K. Nonlinear atom interferometer surpasses classical precision limit. *Nature* **464**, 1165–1169 (2010).
12. Riedel, M. F. et al. Atom-chip-based generation of entanglement for quantum metrology. *Nature* **464**, 1170–1173 (2010).
13. Schleier-Smith, M. H., Leroux, I. D. & Vuletić, V. Squeezing the collective spin of a dilute atomic ensemble by cavity feedback. *Phys. Rev. A* **81**, 021804 (2010).
14. Leroux, I. D., Schleier-Smith, M. H. & Vuletić, V. Implementation of cavity squeezing of a collective atomic spin. *Phys. Rev. Lett.* **104**, 073602 (2010).
15. Kruse, I. et al. Improvement of an atomic clock using squeezed vacuum. *Phys. Rev. Lett.* **117**, 143004 (2016).
16. Pezzè, L., Smerzi, A., Oberthaler, M. K., Schmied, R. & Treutlein, P. Quantum metrology with nonclassical states of atomic ensembles. *Rev. Mod. Phys.* **90**, 035005 (2018).
17. Cox, K. C., Greve, G. P., Weiner, J. M. & Thompson, J. K. Deterministic squeezed states with collective measurements and feedback. *Phys. Rev. Lett.* **116**, 093602 (2016).
18. Hosten, O., Engelsen, N. J., Krishnakumar, R. & Kasevich, M. A. Measurement noise 100 times lower than the quantum-projection limit using entangled atoms. *Nature* **529**, 505–508 (2016).
19. Bohnet, J. G. et al. Quantum spin dynamics and entanglement generation with hundreds of trapped ions. *Science* **352**, 1297–1301 (2016).
20. Braverman, B. et al. Near-unitary spin squeezing in Yb 171. *Phys. Rev. Lett.* **122**, 223203 (2019).

21. Wcisło, P. et al. New bounds on dark matter coupling from a global network of optical atomic clocks. *Sci. Adv.* **4**, eaau4869 (2018).
22. Safronova, M. S. et al. Search for new physics with atoms and molecules. *Rev. Mod. Phys.* **90**, 025008 (2018).
23. Safronova, M. S. The search for variation of fundamental constants with clocks. *Ann. Phys.* **531**, 1800364 (2019).
24. Lisdat, C. et al. A clock network for geodesy and fundamental science. *Nat. Commun.* **7**, 12443 (2016).
25. Grotti, J. et al. Geodesy and metrology with a transportable optical clock. *Nat. Phys.* **14**, 437–441 (2018).
26. Takamoto, M. et al. Test of general relativity by a pair of transportable optical lattice clocks. *Nat. Photon.* **14**, 411–415 (2020).
27. Kolkowitz, S. et al. Gravitational wave detection with optical lattice atomic clocks. *Phys. Rev. D* **94**, 124043 (2016).
28. Wineland, D. J., Bollinger, J. J., Itano, W. M. & Heinzen, D. J. Squeezed atomic states and projection noise in spectroscopy. *Phys. Rev. A* **50**, 67–88 (1994).
29. Kitagawa, M. & Ueda, M. Squeezed spin states. *Phys. Rev. A* **47**, 5138–5143 (1993).
30. Hamley, C. D., Gerving, C., Hoang, T., Bookjans, E. & Chapman, M. S. Spin-nematic squeezed vacuum in a quantum gas. *Nat. Phys.* **8**, 305–308 (2012).
31. Leroux, I. D., Schleier-Smith, M. H. & Vuletić, V. Orientation-dependent entanglement lifetime in a squeezed atomic clock. *Phys. Rev. Lett.* **104**, 250801 (2010).
32. Wineland, D. J. et al. Experimental issues in coherent quantum-state manipulation of trapped atomic ions. *J. Res. Natl. Inst. Stand. Technol.* **103**, 259–328 (1998).
33. Braverman, B., Kawasaki, A. & Vuletić, V. Impact of non-unitary spin squeezing on atomic clock performance. *New J. Phys.* **20**, 103019 (2018).
34. Matei, D. G. et al. 1.5μm lasers with sub-10 MHz linewidth. *Phys. Rev. Lett.* **118**, 263202 (2017).
35. Hu, L., Poli, N., Salvi, L. & Tino, G. M. Atom interferometry with the Sr optical clock transition. *Phys. Rev. Lett.* **119**, 263601 (2017).
36. Pospelov, M. et al. Detecting domain walls of axionlike models using terrestrial experiments. *Phys. Rev. Lett.* **110**, 021803 (2013).
37. Riehle, F. Optical clock networks. *Nat. Photon.* **11**, 25–31 (2017).
38. Al-Masoudi, A., Dörscher, S., Häfner, S., Sterr, U. & Lisdat, C. Noise and instability of an optical lattice clock. *Phys. Rev. A* **92**, 063814 (2015).

Methods

Loading of atoms into two-dimensional magical-wavelength optical lattice

The experimental sequence starts with loading ^{171}Yb atoms into a two-colour mirror magneto-optical trap (MOT) on the singlet $^1S_0 \rightarrow {}^1P_1$ and triplet $^1S_0 \rightarrow {}^3P_1$ transitions, followed by a second-stage green MOT on the triplet transition. By changing the magnetic field, the atomic cloud is then transported into the intersection region of the cavity TEM_{00} mode and a one-dimensional optical lattice along the x direction (see Fig. 1). The trap is formed by 'magic-wavelength' light with $\lambda_t \approx 759$ nm, and the trap depth is $U_x = k_B \times 10$ μK (k_B, Boltzmann constant). The green MOT light is then turned off, and the magic-wavelength trap inside the cavity, detuned from the x lattice by 160 MHz to avoid interference, is ramped up in 40 ms to a trap depth of $U_c = k_B \times 120$ μK. At the end of the loading process, the transverse lattice power is ramped down to zero and back to full power in 50 ms to remove all the atoms that are outside the overlap region of the two lattices. In this way, an ensemble of typically $N = 350$ atoms is prepared at a distance of 370 μm from the end mirror of the cavity. At this location, the single-atom peak cooperativity is $\eta_0 = 3.1$ (ref. [39]).

Raman sideband cooling

After loading the atoms into the two-dimensional optical lattice, the atomic temperature is typically 10 μK, as measured by sideband spectroscopy of the clock transition $^1S_0 \rightarrow {}^3P_0$ (ref. [40]). Subsequently, Raman sideband cooling is performed on the transition $^1S_0 \rightarrow {}^3P_1$ in an applied magnetic field of $B_z = 13.6$ G along the z direction. In 100 ms, the atomic temperature is lowered to 1.8 μK, corresponding to an average motional occupation number of $\langle n_x \rangle = 0.2$ at a trap vibration frequency of $\omega_x/(2\pi) = 67$ kHz along the x direction. The cavity trap is then adiabatically ramped down to $U_c = k_B \times 40$ μK to further reduce the temperature and lower the rate at which atoms in the $^3P_0$ state scatter trap light. We observe that during the Raman sideband cooling, where the optical pumping is provided by intracavity light, the atoms reorganize along the lattice so that all atoms have nearly the maximum coupling η_0 to the cavity mode and the squeezing light.

State measurement

The final measurement of S_z is performed in the ground-state manifold. It is obtained from the difference $S_z = (N_\uparrow - N_\downarrow)/2$ of the populations $N_\uparrow$ and $N_\downarrow$ of the states $|\uparrow\rangle = |{}^1S_0, m_F = +1/2\rangle$ and $|\downarrow\rangle = |{}^1S_0, m_F = -1/2\rangle$, respectively. We first measure $N_\uparrow$ through the vacuum Rabi splitting of the cavity mode $2g \approx \sqrt{N_\uparrow \eta \kappa \Gamma}$ when the empty cavity is resonant with the transition $|\uparrow\rangle \rightarrow |{}^3P_1; F = 3/2, m_F = +3/2\rangle$ (refs. [20,41]). Here $\eta = 3.12(5)$ is the effective single-atom cooperativity, $\kappa = 2\pi \times 520(10)$ kHz is the cavity linewidth and $\Gamma = 2\pi \times 184(1)$ kHz the linewidth of the atomic transition. The Rabi splitting is measured by scanning the laser frequency and detecting the cavity transmission as a function of the frequency. After that measurement, we apply an RF π pulse to switch the populations of $|\uparrow\rangle$ and $|\downarrow\rangle$. The resulting Rabi splitting of the cavity mode is now proportional to $N_\downarrow$. We then perform a second measurement, starting with $N_\downarrow$ to account for atom loss during detection[20], and average the two results according to the formula $S_z = (S_z^{(1)} + S_z^{(2)})/2 = (N_\uparrow^{(1)} - N_\downarrow^{(1)} - N_\downarrow^{(2)} + N_\uparrow^{(2)})/4$. The measurement resolution, expressed in variance normalized to the SQL, is given by $\sigma_d^2 = 2\mathrm{var}(S_z^{(2)} - S_z^{(1)})/N$, where $S_z^{(i)} = (N_\uparrow^{(i)} - N_\downarrow^{(i)})/2$. Our measurement resolution is $\sigma_d^2 = 0.125$ (ref. [20]). Given that all atoms have the same coupling to the cavity, the atom number N inferred from the Rabi splitting equals the real number of atoms in the cavity.

Contrast measurement

Our goal here is to discriminate loss of coherence between atoms (a change of length of the total spin vector $|\langle \mathbf{S} \rangle|$, from dephasing between the atomic spin vector $\mathbf{S}$ and the local oscillator. The latter dephasing is dominated by local-oscillator phase noise and is the signal that we want to measure (and feed back) when operating the system as a full atomic clock. Processes that induce loss of coherence between atoms include magnetic-field gradients, atom–atom collisions and light scattering by the atoms.

For coherent states and squeezed states with low antisqueezing, the length of the atomic spin vector $|\langle \mathbf{S} \rangle|$ can be determined even in the limit where the local-oscillator phase noise is much larger than 2π. If we perform many measurements with homogeneously randomly distributed Ramsey phases ϕ_R, then the variance of the variable $S_z = |\langle \mathbf{S} \rangle| \cos\phi_R$ is

$$(\Delta S_z)^2 = \frac{|\langle \mathbf{S} \rangle|^2}{2\pi} \int_0^{2\pi} \cos^2\phi_R \, \mathrm{d}\phi_R = \frac{|\langle \mathbf{S} \rangle|^2}{2}.$$

We can thus infer the length $|\langle \mathbf{S} \rangle|$ of the mean spin vector by measuring the variance of the outcomes of a Ramsey sequence.

Local-oscillator laser

The local-oscillator laser deployed here is a distributed feedback laser diode operating at a wavelength of 1,157 nm. It uses a fibre-coupled electro-optic modulator (EOM) inside the optical feedback path[42], allowing to control the laser frequency with high gain and a large bandwidth. The primary laser is pre-stabilized to a highly stable, high-finesse optical cavity using a standard Pound–Drever–Hall frequency stabilization scheme. The light is used to inject a gain chip to increase the power, and the output of the secondary laser is frequency-doubled to reach the optical-clock transition wavelength of 578 nm.

Local-oscillator noise

The local-oscillator noise is characterized by interrogating the atoms. We perform a standard Ramsey sequence every 4 s and measure the variance $(\Delta\phi)^2$ of the accumulated phase for different Ramsey times τ_R.

We first find that the noise is uncorrelated between different sequences. This is based on a Ljung–Box test performed after removal of long-time drifts (>30 s). Moreover, we observe that the phase variance scales quadratically with τ_R, indicating that the local-oscillator noise is dominated by very-low-frequency components $f \approx 1/T_c$. For $T_c \gg \tau_R$ we model the atom–local-oscillator phase variance as

$$(\Delta\phi)^2 = (\Delta\omega)^2 \tau_R^2 + \frac{\xi_W^2}{N}, \qquad (2)$$

where $(\Delta\omega)^2$ is the sequence-to-sequence angular frequency variance of the local oscillator, and ξ_W^2/N is the total projection noise induced by N atoms. With a CSS input, our system has a Wineland parameter of $\xi_W^2 = 1.35$ (see Fig. 3). By fitting the data with the model we obtain $\Delta\omega = 2\pi \times (78 \pm 3)$ Hz. With the cycle time $T_c = 4$ s of our system, we infer a local-oscillator-noise-induced clock short-term fractional stability of $\sigma_{LO} = 3 \times 10^{-13} \tau^{-1/2}$. This result is in good agreement with the expected Dick noise calculated with equation 8 in ref. [38] and assuming a realistic single-sided local-oscillator spectral power density composed by flicker ($1/f$) and Brown ($1/f^2$) noise components.

For a Ramsey time of $\tau_R = 1.16$ ms, a CSS Wineland parameter of $\xi_W^2 = 1.35$ and $N = 300$, the projection noise contribution to the fractional stability is $\sigma_{PN} = 3 \times 10^{-14} \tau^{-1/2}$, and therefore negligible compared to the local-oscillator noise contribution. Moreover, for a Ramsey time of $\tau_R = 0.17$ ms and the same atom number, we have $\sigma_{PN} \approx \sigma_{LO}$.

We define the local-oscillator coherence time τ_{LO} as the Ramsey time for which the local-oscillator noise standard deviation, including Dick noise, reaches $\Delta\phi(\tau_{LO}) = \pi/2$. This results in $\tau_{LO} = (\pi/2)/\Delta\omega = 6$ ms for our current system.

Local-oscillator noise subtraction

As discussed in the previous section, the sequence with longer Ramsey time ($\tau_{R2} = 1.16$ ms) allows us to directly measure the total noise coming

from the local oscillator. In Fig. 4a the self-referenced Allan deviation of the local-oscillator noise is fitted to the model $A/\sqrt{\tau}$, with $A = 3.0(1) \times 10^{-13}\ s^{1/2}$. Owing to the very low duty cycle and the noise spectral distribution of our local oscillator, the contribution of Dick noise to the measurement is the same for both Ramsey times (that is, 1.16 ms and 0.17 ms). In Fig. 4a we plot the self-referenced Allan deviations of the short Ramsey time sequences from which we subtract the fitted local-oscillator noise in quadrature to obtain Fig. 4c.

Potential systematic effects

We do not expect any major systematic effects when using an SSS instead of a CSS in future systems, which will be able to reach fractional accuracies as low as 10^{-19}. However, we foresee the appearance of some effects due to the presence of the cavity; nonetheless, these effects can be controlled and removed. One potential issue would be the electric-field noise generated by charges present in the micro-mirror substrate. However, with another cavity design—for example, a bow-tie cavity—it would be possible to reach similar or higher atom–cavity cooperativities while keeping the atomic ensemble several centimeters away from mirrors, comparable to other dielectrics in present OLCs. The cavity can also induce a Lamb shift of the clock transition during the Ramsey time owing to the virtual emission and reabsorption of a photon for atoms in the upper $^3P_0$ clock state. This can be controlled during the Ramsey time either by adjusting the cavity length so that the cavity modes are detuned symmetrically from the atomic resonance, or by moving the atoms outside the cavity mode during the Ramsey time, for example, by means of a moving standing wave of trapping light.

Improving local-oscillator laser stability

Our local-oscillator laser performance is limited by low-frequency mechanical vibrations, residual amplitude modulation (RAM) noise, as well as flicker-type noise such as Brownian noise. In order to reach relevant local-oscillator linewidths and phase coherence times that allow for second-scale interrogation times, various sources of technical noise must be substantially reduced. RAM noise in the Pound–Drever–Hall lock to an ultrastable cavity can be reduced by up to 60 dB by active feedback acting directly on the EOM[43]. Similarly, the effective fibre length and phase noise can be stabilized by well studied interferometric schemes as in ref. [44]. Furthermore, our local oscillator stabilized to a state-of-the-art ultralow-expansion cavity in a temperature- and vibration-stabilized housing should reach a thermal-noise-limited stability of 5×10^{-17} (ref. [45]), enabling a clock with Ramsey time up to 5 s.

Data availability

All data obtained in the study are available from the corresponding author upon reasonable request.

39. Kawasaki, A. et al. Geometrically asymmetric optical cavity for strong atom-photon coupling. *Phys. Rev. A* **99**, 013437 (2019).
40. Blatt, S. et al. Rabi spectroscopy and excitation inhomogeneity in a one-dimensional optical lattice clock. *Phys. Rev. A* **80**, 052703 (2009).
41. Vallet, G. et al. A noise-immune cavity-assisted non-destructive detection for an optical lattice clock in the quantum regime. *New J. Phys.* **19**, 083002 (2017).
42. Yamoah, M. et al. Robust kHz-linewidth distributed Bragg reflector laser with optoelectronic feedback. *Opt. Express* **27**, 37714–37720 (2019).
43. Zhang, W. et al. Reduction of residual amplitude modulation to 1×10^{-6} for frequency modulation and laser stabilization. *Opt. Lett.* **39**, 1980–1983 (2014).
44. Śliwczyński, Ł., Krehlik, P., Czubla, A., Buczek, Ł. & Lipiński, M. Dissemination of time and RF frequency via a stabilized fibre optic link over a distance of 420 km. *Metrologia* **50**, 133 (2013).
45. Lee, W. et al. Ultrastable laser system using room-temperature optical cavity with 4.8×10^{-17} thermal noise limit. In *2019 Joint Conference of the IEEE International Frequency Control Symposium and European Frequency and Time Forum* 1–2 (IEEE, 2019).

Acknowledgements We thank H. Katori, W. Ketterle, A. Ludlow, M. Lukin, J. Ramette, G. Roati, A. Urvoy, Z. Vendeiro and J. Ye for discussions. This work was supported by NSF, DARPA, ONR and the NSF Center for Ultracold Atoms (CUA). S.C. and A.F.A. acknowledge support from the Swiss National Science Foundation (SNSF). B.B. acknowledges support from the National Science and Engineering Research Council of Canada.

Author contributions A.K., B.B., C.S., E.P.-P., S.C., A.F.A., Z.L., E.M. and V.V. contributed to the building of the experiment. E.P.-P., S.C. and C.S. led the experimental efforts and simulations. S.C., A.F.A., C.S. and E.P.-P. contributed to the data analysis. V.V. conceived and supervised the experiment. S.C. and V.V. wrote the manuscript. All authors discussed the experiment implementation and results and contributed to the manuscript.

Competing interests The authors declare no competing interests.

Additional information
Supplementary information is available for this paper at https://doi.org/10.1038/s41586-020-3006-1.
Correspondence and requests for materials should be addressed to V.V.
Peer review information *Nature* thanks the anonymous reviewer(s) for their contribution to the peer review of this work. Peer reviewer reports are available.
Reprints and permissions information is available at http://www.nature.com/reprints.